Capillarity

Vol. 14, No. 3, p. 72-81, 2025

Original article

Wetting behaviors of water on kerogen surfaces from molecular level: Implication for gas extraction and hydrogen storage in shale

Mingshan Zhang[1]*, Jinsong Huang[2], Han Wang[3], Wente Niu[1]*

[1]School of Vehicle and Energy, Yanshan University, Qinhuangdao 066000, P. R. China
[2]CNOOC EnerTech-Drilling & Production Co., Tianjin 300452, P. R. China
[3] National Key Laboratory of Petroleum Resources and Engineering, China University of Petroleum, Beijing 102249, P. R. China

Keywords:
Wettability
shale gas
kerogen
hydrogen storage
Young-Laplace equation

Cited as:
Zhang, M., Huang, J., Wang, H., Niu, W. Wetting behaviors of water on kerogen surfaces from molecular level: Implication for gas extraction and hydrogen storage in shale. Capillarity, 2025, 14(3): 72-81. https://doi.org/10.46690/capi.2025.03.02

Abstract:
Shale formations serve as primary reservoirs for natural gas and emerging candidates for hydrogen storage, where the wetting behaviors of organic matter (i.e., kerogen) play a critical role in fluid retention and transport. This study employed molecular dynamics simulations to investigate the pressure-dependent wettability of kerogen surfaces in H_2 and CH_4 environments under geological conditions (333 K, 10-100 MPa). Results reveal distinct gas-specific mechanisms governing wettability evolution. For CH_4-H_2O systems, increasing pressure induces a wettability transition from weakly water-wet to gas-wet due to the strong interaction between CH_4 and the kerogen surfaces, which results in a smaller gas-solid interfacial tension compared with liquid-solid interfacial tension . Meanwhile, both the reduced gas-liquid and gas-solid interfacial tension contributes to a linear rise in contact angles (88° to 119°). In contrast, H_2 exhibits weaker interactions with the kerogen surfaces and experiences a minimal decrease in gas-liquid interfacial tension, thus presenting persistently water-wet characteristics (53° to 69.5°) even at 100 MPa. Crucially, the Young-Laplace equation remains valid at the nanoscale, as evidenced by direct capillary pressure measurements aligning with theoretical predictions, confirming classical interfacial thermodynamics govern nanoconfined fluid behavior. These mechanistic insights elucidate how gas-specific molecular interactions dictate shale wettability, providing a physicochemical basis for optimizing CH_4 recovery through pressure-managed wettability alteration and ensuring H_2 storage security in hydrophobic kerogen network.

1. Introduction

Wettability, governing fluid adhesion and displacement at solid interfaces, is a pivotal factor in subsurface engineering systems, from CH_4 recovery to geo-storage of gases like H_2 (Iglauer et al., 2021; Pan et al., 2022). In geological formations, surface wetting properties dictate capillary forces that affect structural trapping efficiency, fluid mobility, and storage security-parameters critical for both energy extraction and decarbonization efforts (Krishnamurthy et al., 2022). Shale formation naturally serves dual roles as prevalent CH_4 hosts and potential H_2 storage sites, in which kerogen is widely distributed (up to 30 vol% in total) (Al-Yaseri et al., 2022; Jagadisan and Heidari, 2022; Wang et al., 2024a). Kerogen, a macromolecular organic phase, is characterized as well-

---

*Corresponding author.

E-mail address: zhangms@ysu.edu.cn (M. Zhang); saww0218@gmail.com (J. Huang); hanwang@cup.edu.cn (H. Wang); wentn24@ysu.edu.cn (W. Niu).

Yandy Scientific Press

2709-2119

Received January 29, 2025; revised February 22, 2025; accepted March 15, 2025; available online March 18, 2025.

developed nanopores, where the capillary effect is significant (Chalmers and Bustin, 2017). The wettability of kerogen surfaces plays a key role in gas retention manners in shale media, and it dynamically changes with gas species and pressures (Pan et al., 2020). Therefore, a fundamental understanding of wettability behaviors of kerogen in shale is crucial for optimizing CH_4 recovery while enabling safe H_2 storage.

Surface wettability is fundamentally characterized by the contact angle (CA), a geometric parameter defined at the three-phase boundary where liquid, gas, and solid intersect (Huhtamäki et al., 2018). This metric is thermodynamically governed by Young's equation, which balances interfacial tensions across solid-vapor, liquid-vapor, and solid-liquid interfaces (Young, 1805). Experimentally, CA is quantified using techniques such as sessile drop, captive bubble, Wilhelmy plate, and tilting plate methods (Lander et al., 1993; Hashemi et al., 2021; Alhamad et al., 2023; Kuthe et al., 2025). For porous media like shale rocks, spontaneous imbibition tests and nuclear magnetic resonance spectroscopy further provide indirect wettability assessments by correlating fluid saturation dynamics or surface relaxation rates with interfacial affinity (Alinejad and Dehghanpour, 2021; Wang et al., 2024b).

Current understanding of shale wettability predominantly stems from experimental studies on organic-rich shale samples, while investigations targeting isolated kerogen remain scarce due to technical difficulties in extracting pure organic matter from mineral matrices (Suekuni et al., 2022). Shales typically exhibit mixed-wet behavior arising from their heterogeneous mineralogy: hydrophilic phases (e.g., quartz, carbonates) coexist with hydrophobic kerogen networks (Li et al., 2023). Experimental investigations under various gas environments (CH_4, CO_2, H_2) have identified total organic carbon brine salinity, and pore geometry as key factors governing wettability, where elevated total organic carbon and ionic strength typically promote the hydrophobicity of shale rocks (Pan et al., 2018; Qin et al., 2022; Zheng et al., 2024). Despite these advances, macroscopic measurements often fail to reveal the atomic-scale mechanisms controlling fluid spreading on kerogen surfaces. More importantly, experimental uncertainties persist due to confounding factors such as surface roughness artifacts, trace mineral contaminants in isolates, and heterogeneity of sample surfaces.

Molecular dynamics (MD) simulations serve as a critical complement to experimental approaches, enabling atomic-level insights into wettability mechanisms by precisely controlling surface chemistry and decoupling interfacial interactions. For instance, Zhou et al. (2022) demonstrated that CO_2-induced suppression of hydrogen bonding between water and polar groups shifts wettability from water-wet to CO_2-wet at elevated pressures. Similarly, Jagadisan and Heidari (2022) linked decreasing water wettability with kerogen maturation to rising aromaticity and declining O/C ratios, while Yang et al. (2023) quantified opposing effects of H_2 pressure (increasing CA) and temperature (decreasing CA) in kerogen/H_2/water systems. Notably, Sanchouli et al. (2024) highlighted the non-trivial roles of nanoscale droplet size, surface roughness, and kerogen model rigidity in modulating apparent contact angles. Yan et al. (2025) used MD simulations to study the spread radius and contact angle of water on kerogen surfaces at various CO_2 pressures. They found that the wettability of kerogen substrate gradually transitioned from intermediate-wet to strongly CO_2-wet as CO_2 pressure increased.

While previous studies have advanced our understanding of kerogen wettability under CO_2 environments and general gas conditions, critical gaps remain in comparing shale gas (CH_4) and hydrogen (H_2) storage systems. Existing MD simulations predominantly focus on single-gas scenarios or maturation effects, lacking systematic investigations of pressure-dependent wettability transitions between these functionally distinct gas species. Furthermore, the nanoscale validity of Young-Laplace theory-a cornerstone for predicting capillary pressures in conventional reservoirs-remains unverified for kerogen nanopores under hydrogen exposure. To address these limitations, MD simulations were conducted to quantify gas-specific wettability trends of water on kerogen surfaces across geological pressure conditions (10-100 MPa at 333 K) and elucidated fundamental mechanisms driving divergent CH_4-H_2O and H_2-H_2O interfacial behaviors through adsorption layer analysis. More importantly, the applicability of Young-Laplace was rigorously tested at nanoscopic dimensions via novel gas expansion simulations. This work provides important insights into water wettability on kerogen when immersed in CH_4 or H_2, revealing a critical pressure threshold (30 MPa) where CH_4 systems transition from water-wet to gas-wet states while H_2 environments maintain water affinity. These insights directly inform shale gas recovery strategies by identifying pressure windows for optimal capillary-driven CH_4 release, while establishing hydrogen storage safety criteria through quantified water invasion risks in kerogen nanopores.

2. Methodology

2.1 Molecular model

Kerogens II-A, II-B, II-C, and II-D represent oil-prone organic matter deposited in marine anoxic environments, serving as the most prolific source of conventional hydrocarbons in major oil provinces worldwide, including the Middle East, the northern North Sea (Kimmeridge Clay and Draupne Formations), and western Canada (Ungerer and Yiannourakou, 2015). Overmature Type II kerogen, exemplified by II-D, is representative organic matter in unconventional shale gas reservoirs such as the Barnett Shale, where advanced thermal maturity drives gas generation. As this study focuses on shale gas reservoirs, the molecular model of Type II-D kerogen unit was adopted to represent shale organic matter in this study (Ungerer and Yiannourakou, 2015). This model has been extensively validated against experimental benchmarks for gas-mature shales, including elemental stoichiometry, aromaticity, and heteroatom distribution, ensuring its accuracy in reproducing petro-chemical properties critical for subsurface wettability simulations. The construction of kerogen matrix includes four stages, combining molecular templating and annealing techniques. Firstly, two monolayer graphene sheets ($x-y$ dimensions: 20.42×8.105 nm^2) were constructed using the Visual Molecular Dynamics package. These sheets were vertically aligned along the z-axis, with positions fixed at z

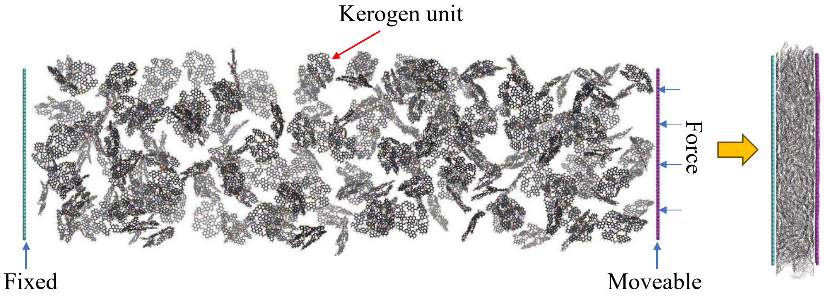

Fig. 1. Construction diagram of kerogen substrate model. Color scheme: Black, C in kerogen; Red, O; Yellow, S; Blue, N; Purple and Cyan, C in graphene sheet.

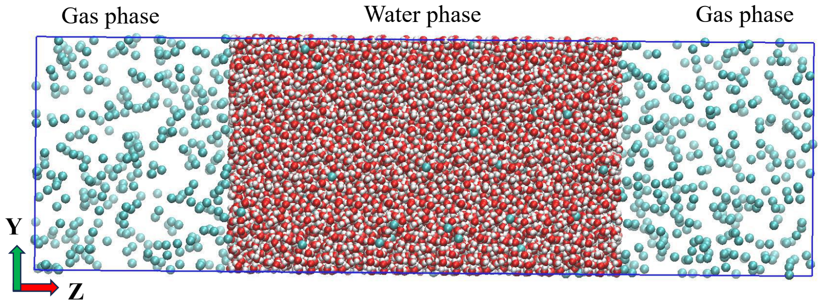

Fig. 2. Gas-water two phase slab molecular model for IFT calculation.

= 0 nm (base) and z =100 nm (top). Then, 180 Type II-D kerogen units were randomly inserted into the graphene-confined space using PACKMOL (see Fig. 1). Subsequently, the system underwent staged annealing under the NVT ensemble. Meanwhile, a constant external acceleration (-0.3 nm/ps^2) was applied to the upper graphene sheet to compress the kerogen molecules, while the base sheet remained fixed. The acceleration value serves as a recommended baseline rather than a fixed parameter. Reasonable results are achieved by adjusting it within a practical range to maintain adequate kerogen surface smoothness, while avoiding excessively low values. Finally, the graphene templates were removed resulting in a kerogen matrix with a relative smooth surface. The consistent valence force field is adopted to describe kerogen, which has been widely used to study wetting behaviors of kerogen substrate (Hagler and Dauber, 1979). CH_4 and H_2O molecules were simulated by the TraPPE-UA, and OPC4 force field, respectively. The settle algorithm was applied to constrain the rigid geometry of water molecules (Miyamoto and Kollman, 1992; Potoff and Siepmann, 2001; Izadi et al., 2014).The four-site water model demonstrates superior accuracy to conventional three-site models (TIP3P, SPC/E) in replicating key thermodynamic and dynamic properties of bulk water. Notably, it provides more reliable predictions of surface tension (a critical parameter for reproducing the wettability of water), which three-site models underestimate by approximately 28% (Kadaoluwa Pathirannahalage et al., 2021; Tempra et al., 2022). A three-site model is used to simulate H_2, as it can better reflect the quadrupole moment of H_2 (Alavi et al., 2005).

2.2 Force field calibration

Force field validation was performed through systematic benchmarking of MD-derived thermophysical properties against NIST reference data and experimental datasets, focusing on gas-phase bulk densities and water-gas interfacial tension (IFT). The bulk gas density is obtained by performing an NPT (constant particle number, pressure, and temperature) simulation at specific temperature and pressure conditions. For IFT calculations, a dual-phase slab model with a cross-section 6.0 × 6.0 nm^2 (see Fig. 2) was equilibrated under NPT conditions.

The IFT values (σ) are computed via (Kirkwood and Buff, 1949):

$$\sigma = (< P_{zz} > - \frac{< P_{xx} > + < P_{yy} >}{2}) \times \frac{L_z}{2} \tag{1}$$

where L_z is the average length of the simulation box in z direction, and $<P_{\alpha\alpha}>$ ($\alpha = x, y, z$) denotes time ensemble-average diagonal pressure tensor components. To reconcile discrepancies in CH_4-H_2O systems, cross-interaction parameters were optimized by scaling the ε parameter between O atoms in water and CH_4 molecules with a factor of 1.2. As evidenced in Fig. 3, the simulated bulk gas densities and IFT values agree well with the experimental data, showing an excellent reliability of these selected force fields (Chow et al., 2018; Ren et al., 2000).

2.3 Simulation details

A multiphase system (see Fig. 4) containing a cylindrical water droplet (8000 molecules, initial diameter of 3 nm), target gas species (H_2 or CH_4), a kerogen substrate, and a graphene

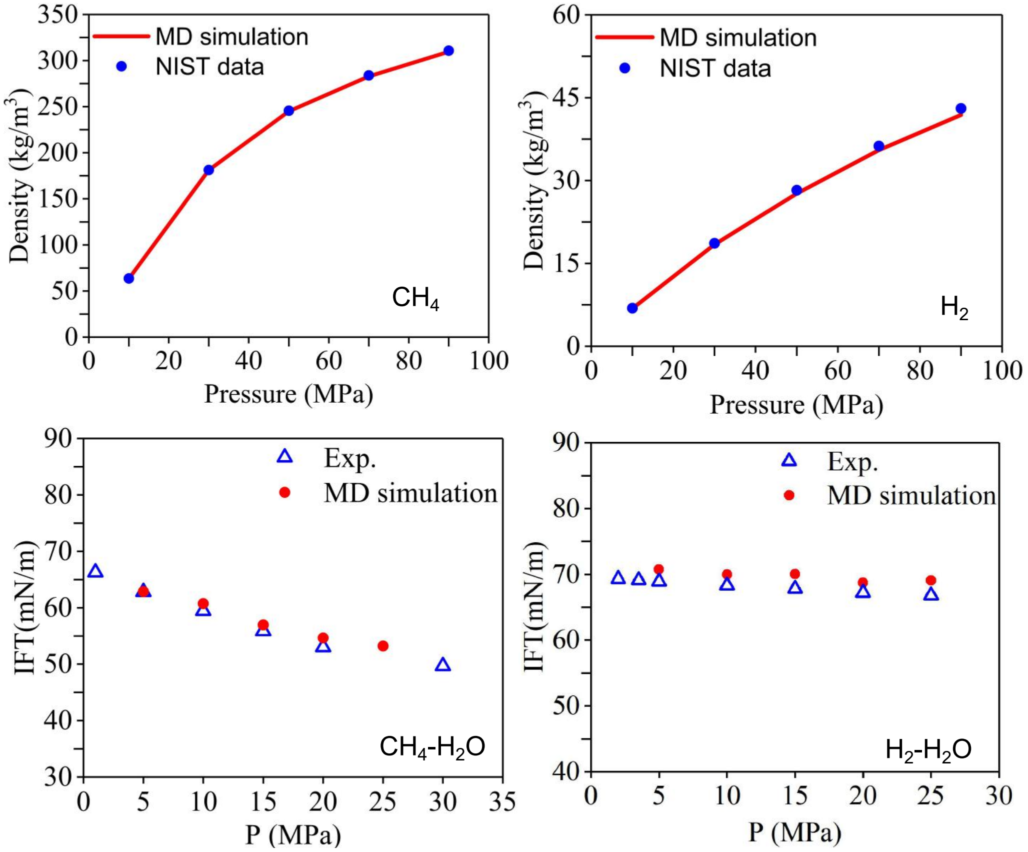

Fig. 3. Force field validation for bulk density and water-gas IFT.

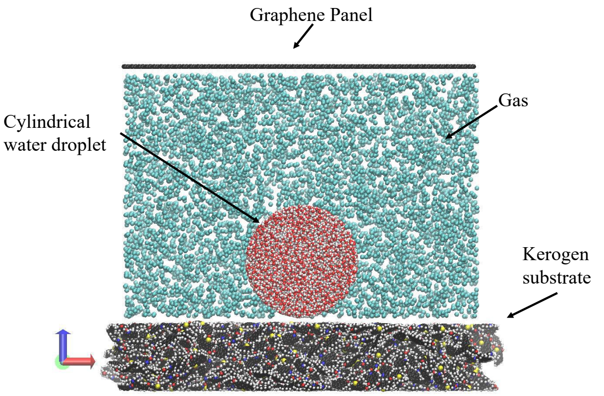

Fig. 4. Schematic representations of initial configuration for wettability simulation system with CH_4 gas.

Table 1. Component details of different simulation systems.

Gas type	Number of gases	Equilibrium pressure (MPa)	Equilibrium CA (°)
CH_4	6500	11	88
	16000	30	97
	21000	50	106
	24200	68	111.5
	26200	88	119
H_2	5200	10	53
	13000	28	60
	19000	44	64
	24200	62	67
	29500	91	69.5

confinement panel was fabricated to investigate the wettability behaviors. The cylindrical-shaped water droplet was used to avoid the line tension effects (Scocchi et al., 2011). On the one hand, the graphene panel is used to prevent gas-kerogen interactions at the periodic boundary. On the other hand, it is useful to add a vacuum layer to minimize the periodic boundary condition effect. Initially, the water droplet was positioned centrally above the quartz surface, and the remaining space is filled with gas molecules. To study the pressure effects, different numbers of gas molecules are placed into the simulation system. Based on the density profile of gas at equilibrium, the system pressure can be determined. a total of 10 simulation scenarios are designed to calculate the CA at various pressure conditions and the detailed system settings were summarized in Table 1 (For all the simulation scenarios, the number of water molecules is set to 8,000).

Using GROMACS package (version 2019.6), the wettability simulations were initiated with energy minimization

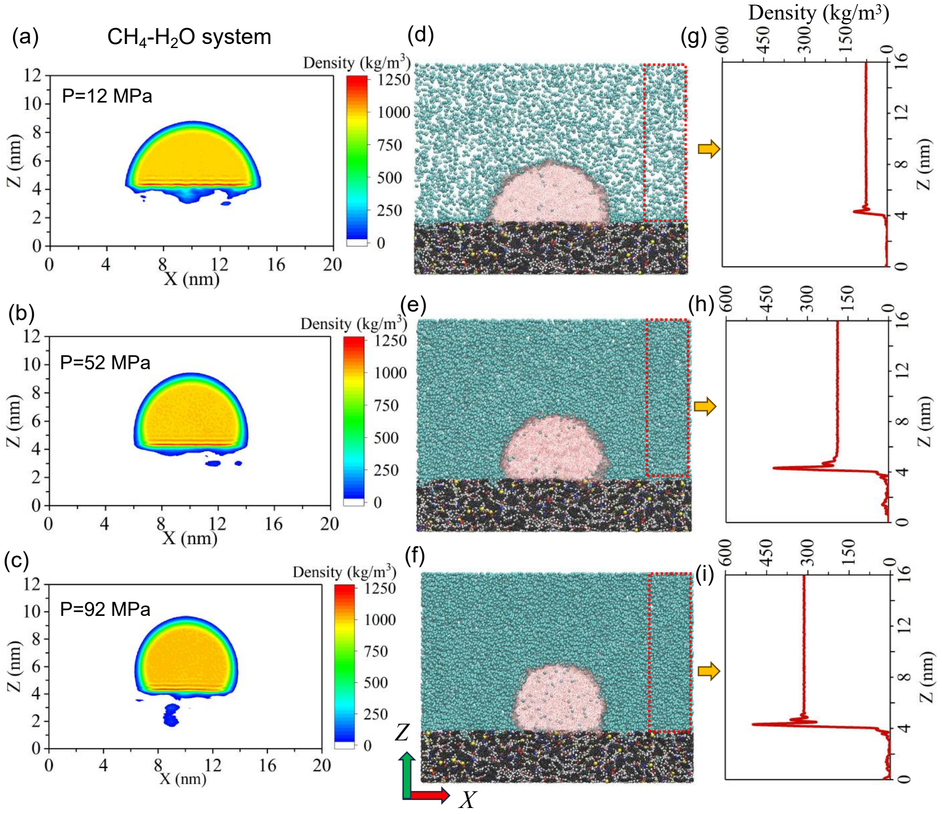

Fig. 5. (a)-(c) 2D density distribution of water, (d)-(f) equilibrated snapshots of water droplet, and (g)-(i) 1D density profile of CH_4 along z direction under different pressure conditions for CH_4-H_2O system.

(steepest descent algorithm) to eliminate atomic overlaps and steric clashes in the initial configuration (Van Der Spoel et al., 2005). Subsequently, a 20-ns NVT (constant particle number, pressure, and volume) ensemble simulation (with a time step of 1 fs) was performed to investigate water droplet spreading behaviors on the kerogen substrate. The simulation temperature was maintained at 333.15K using the v-rescale thermostat (Bussi et al., 2007). The atoms of kerogen substrate are kept frozen throughout the simulation. Nonbonded interactions employed geometric mixing rules for most atom pairs, with optimized cross-interaction parameters for water-CH_4 pairs (as calibrated in Section 2.2). Both Lennard-Jones and Coulombic potentials were truncated at 1.5 nm, complemented by the Particle Mesh Ewald method for long-range electrostatic interaction (Essmann et al., 1995). Three-dimensional periodic boundary conditions were adopted during simulations. Trajectory data from the final 5 ns is used to analyze the equilibrium wetting and distribution behaviors of water and gas molecules.

3. Results and discussions

3.1 Wetting behaviors of water on kerogen surfaces

The 2D density distribution and typical molecular snapshots of water droplets (CH_4-H_2O system) under different simulation pressures after reaching equilibrium are shown in Fig. 5. The 1D density profile of CH_4 presented in the third column is equal to the bulk density, thus it can be used to determine the system pressure. CH_4 forms multiple adsorption layers on kerogen surfaces despite pressure conditions which is in line with previous simulation work (Pang and Jin, 2019). When immersed in CH_4, water droplets demonstrate a reluctant spreading manner on kerogen surfaces, indicating that the affinity between kerogen surfaces and water droplets is not very strong in the presence of CH_4. Meanwhile, as pressure increases from 10 MPa to 92 MPa, the spreading ability of water droplets on the kerogen surfaces is gradually reduced, resulting in a more hydrophobic surface. This transition correlates with pressure-enhanced van der Waals interactions between CH_4 and kerogen's aromatic domains (as evidenced by the augmented first adsorption peak in 1D density profile shown in Figs. 5(g)-5(i)), overriding hydrogen-bonding forces at the water-kerogen interface. Such a wettability transition phenomenon is analogous to CO_2-induced wettability alteration on kerogen surfaces and consistent with the experimental observations (Pan et al., 2018; Zhou et al., 2022).

As demonstrated in Fig. 6, the wetting dynamics of water droplets on kerogen surfaces exhibit marked divergence between H_2-H_2O and CH_4-H_2O systems. In H_2-dominated environments, water droplets display enhanced spreading behavior, yielding lower contact angles that signify persistent water-wet characteristics. This is different from CH_2-H_2O systems, where pressure-dependent hydrophobic transitions occur. The

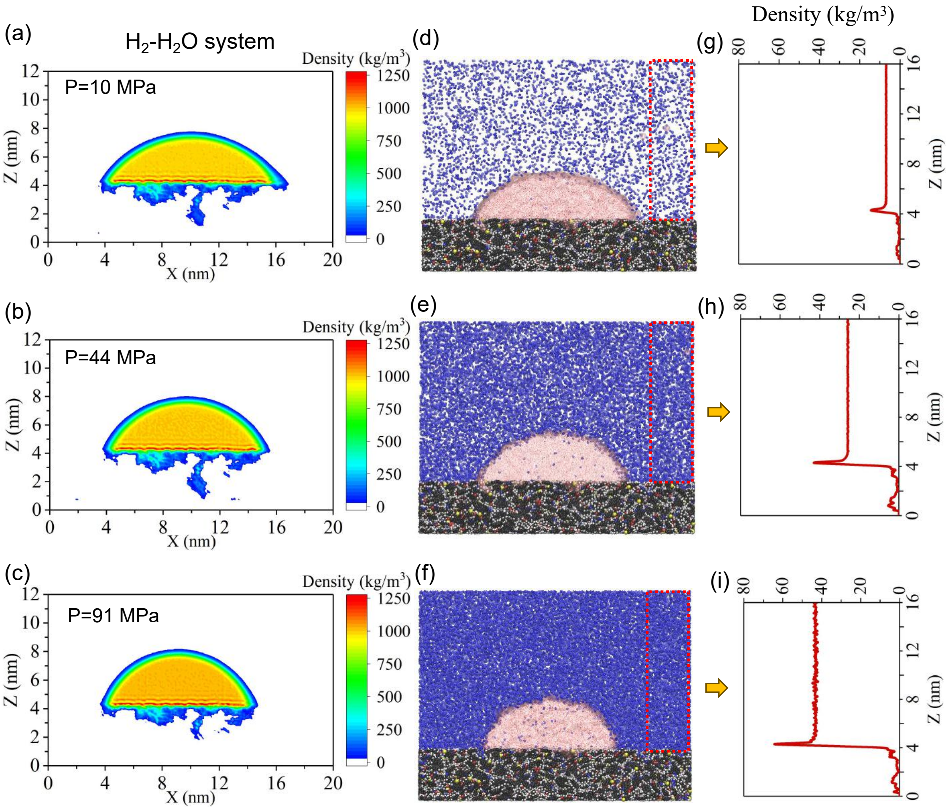

Fig. 6. (a)-(c) 2D density distribution of water, (d-f) equilibrated snapshots of water droplet, and (g-i) density profile of H_2 along z direction under different pressure conditions for H_2-H_2O system.

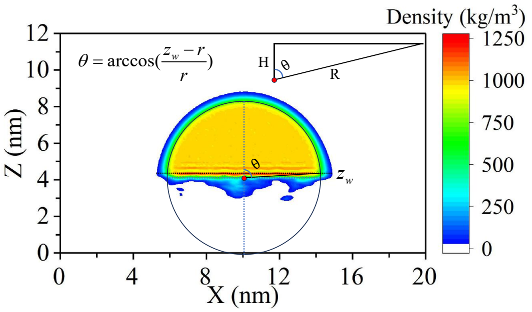

Fig. 7. CA calculation method based on 2D density profile of water.

weakened H_2-kerogen interaction is primarily governed by weaker van der Waals forces compared to CH_2 as also evidenced by the fact that H_2 can only form a single adsorption layer even at extreme pressures (91 MPa).

The wettability of kerogen surfaces, a critical factor governing capillary pressure (CP) via the Young-Laplace (YL) equation, profoundly influences hydrocarbon recovery efficiency and subsurface gas storage security. To quantify this property, the three-phase (water-kerogen-gas) CAs are calculated using a density-based curve fitting method (the detailed calculation formula is illustrated in Fig. 7). Water density profiles, derived from time-averaged molecular trajectories, were mapped into 2D contour plots, where the interfacial boundary was defined by the contour line corresponding to 90% of bulk water density using Origin 2017. An in-house MATLAB algorithm performed least-squares circular fitting on these contour points, generating precise coordinates for the droplet's geometric center and radius (R) of the fitted circle, where the water-kerogen interface (z_w) was identified as the first adsorption peak in the water density profile. The equilibrium CA was then computed geometrically as:

$$\theta = \arccos(\frac{z_w - r}{r}) \tag{2}$$

As is known to all, the relationship between CA and surface tensions can be well described by Young's equation as follows:

$$\cos\theta = \frac{\sigma_{gs} - \sigma_{ls}}{\sigma_{gl}} \tag{3}$$

where σ_{gs}, σ_{ls}, and σ_{gl} are the surface tension of gas-solid, liquid-solid, and gas-liquid interface, respectively. For CH_4-H_2O-kerogen systems, the negative cosθ values (except at pressures < 10 MPa) systematically indicate $\sigma_{gs} < \sigma_{ls}$, thermodynamically preventing water spreading on kerogen surfaces. This phenomenon arises from the strong adsorption affinity of CH_4 to kerogen through van der Waals interactions, effectively reducing the gas-solid interfacial tension. Conversely, in H_2-H_2O-kerogen systems, positive σ_{gs}-σ_{ls} values emerge due to weaker adsorption capacity of kerogen as quantified in our molecular interaction energy analysis, yielding higher σ_{gs} values than CH_4 systems (Huang et al., 2024). Since the interaction between water and kerogen surfaces is insensitive

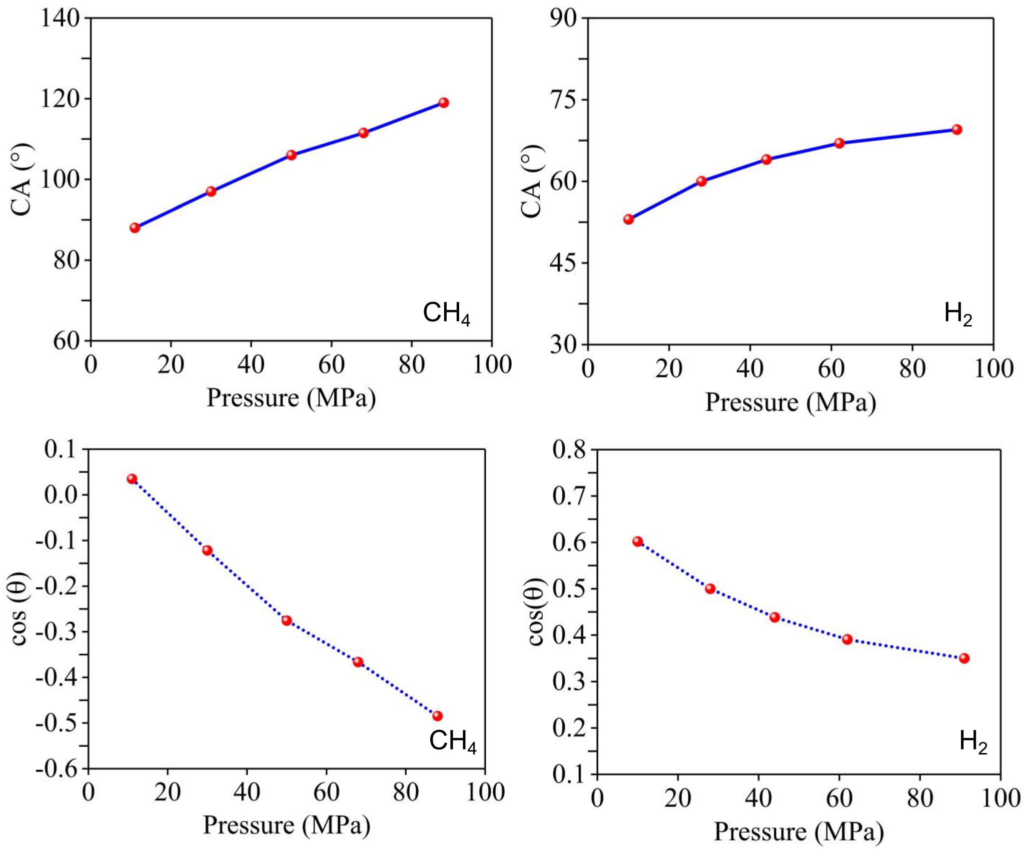

Fig. 8. Variation of CAs and cos(θ) as a function of pressure for CH_4-H_2O and H_2-H_2O systems. The star point is used for capillary pressure calculation with YL equation.

to the pressure, pressure-independent water-kerogen interactions maintain σ_{ls} as a near-constant, making $\cos\theta$ evolution principally governed by σ_{gs} and σ_{gl} variations. For CH_4-H_2O-kerogen systems, as pressure increases, the interaction between CH_4 and the kerogen surfaces is enhanced, leading to a reduced gs, which is unfavorable for increasing liquid-solid interface.

In CH_4 systems, pressure elevation strengthens CH_4-kerogen adsorption (evidenced by increasing CH_4 density peaks near the surface in Fig. 5), progressively lowering σ_{gs}. Concurrently, CH_4-H_2O interfacial tension (σ_{gl}) shows linear pressure-dependent decline (Fig. 3). These dual effects synergistically reduce $\cos\theta$ values and amplify hydrophobicity, driving the wettability transition from water-wet (θ ≈ 88°) to gas-wet (θ ≈ 119°). For H_2 systems, though σ_{gl} also decreases with pressure, limited σ_{gs} variation restricts $\cos\theta$ reduction. This explains why H_2-H_2O-kerogen systems maintains water-wet characteristics ($\theta < 70°$) across the pressure range.

3.2 Applicability of YL equation at nanoscale

The YL equation has been extensively employed for capillary pressure prediction in conventional-scale capillary tubes, yet its applicability at the nanoscale remains scientifically controversial. To address this fundamental question, a novel gas expansion methodology was developed for direct evaluation of capillary forces within kerogen nanopores (4.4 nm pore width) and performed comparative analysis with YL predictions. The pore size is defined as the distance between the closest carbon atoms on two opposite kerogen surfaces. It should be emphasized that our proposed gas-expansion assessment method is fundamentally constrained to water-wet systems by design. Thus, the H_2-H_2O-Kerogen system is applied to test.

The MD simulation operates on this thermodynamic principle: A water column is initially confined at the right-hand extremity of the kerogen nanopore, while the remaining void space is charged with gas (H_2) molecules. The gas quantity is carefully controlled to maintain a pressure marginally exceeding the YL-derived CP estimate, establishing a pressure differential. Through spontaneous thermodynamic equilibration, this pressure gradient drives progressive gas-phase expansion until mechanical equilibrium is achieved (CP = gas pressure), as illustrated in Fig. 9. Throughout this dynamic process, the 2D water distribution map is plotted to track the aqueous phase displacement front (denoted by red markers in Fig. 9), enabling a precise determination of the equilibrium time.

As demonstrated in Fig. 10(a), the aqueous phase displacement front exhibited progressive advancement before reaching thermodynamic equilibrium at the geometric coordinate defined by the intersection of two blue lines. Through quantitative density analysis in Fig. 10(b), the equilibrated gas pressure (i.e., CP) is determined to be 17.0 MPa. Integrating our previously calculated interfacial parameters (H^2-H_2O IFT=

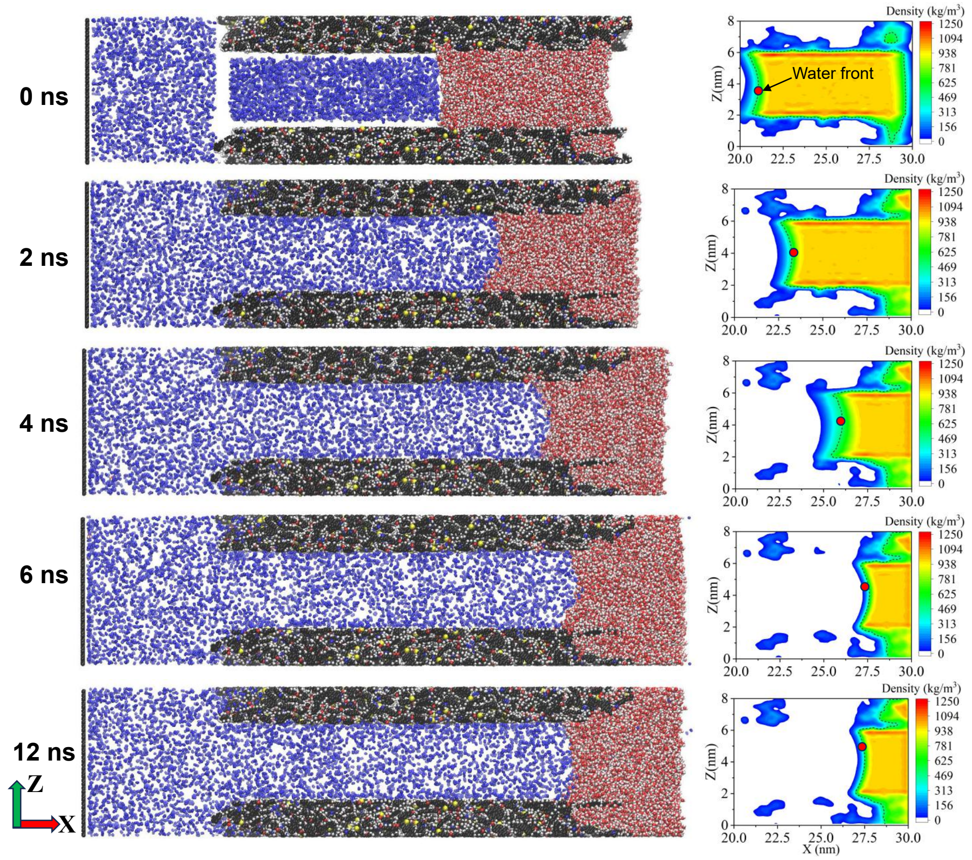

Fig. 9. Dynamic evolution process of H_2 gas expansion and 2D contour map of water at the region circled by yellow dotted lines. The red point in the 2D map represents the front position of the water phase.

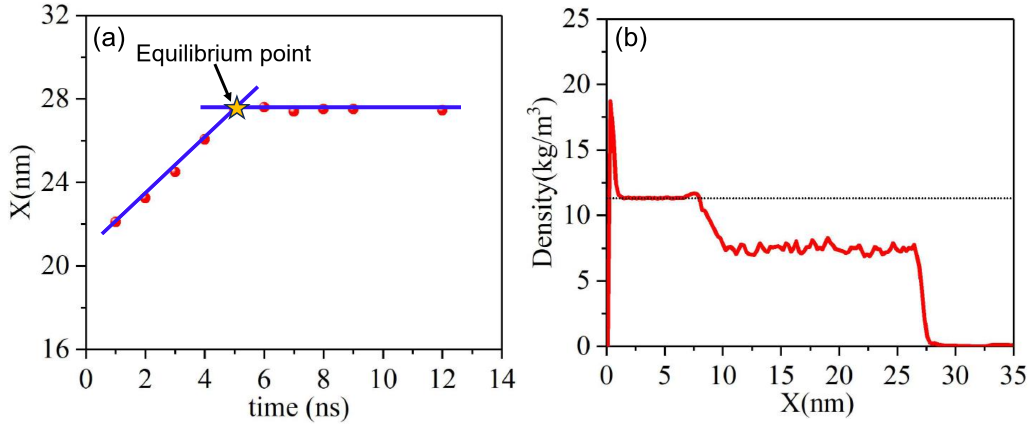

Fig. 10. (a) Variation of water front position as a function of time and (b) equilibrium density profile of H_2 along x direction.

68 mN/m from Fig. 3; CA = 57° from Fig. 8) into the geometrically adapted YL formulation for slit-pore systems:

$$P_c = \frac{2\sigma\cos\theta}{w} \tag{4}$$

where P_c denotes capillary pressure, σ represents interfacial tension, θ is the contact angle, and w corresponds to pore width. The tiny deviation (~1%) of CP between molecular dynamics-derived and the theoretical LP prediction (16.83 MPa vs 17.0 MPa) proves the validity of LP equation in predicating CP within kerogen nanopores.

4. Conclusion

This study employed molecular dynamics simulations to investigate the pressure-dependent wettability of kerogen surfaces in H_2 and CH_4 environments and test the applicability of YL equation at nanoscale. Key findings revealed distinct wetting behaviors between the two gas systems. For CH_4, increasing pressure (10-90 MPa) induces an enhancement in kerogen hydrophobicity, driving a transition from weakly water-wet to gas-wet states. In contrast, H_2 environments maintain water-wet characteristics across the same pressure range, with contact angles stabilizing at ~75° despite rising pressure. These divergent trends stem from differences in gas affinity with kerogen surfaces. The results provide critical molecular-level insights for subsurface engineering applications. The pressure-driven hydrophobicity in CH_4 systems suggests that elevated reservoir pressures could enhance gas mobility and recovery by reducing capillary trapping of water. Conversely, the persistent water-wet behavior in H_2 environments implies favorable conditions for structural trapping of hydrogen in kerogen-rich shales, supporting secure geo-storage strategies. Most importantly, our results proved that the YL equation can also work well when predicting the capillary pressure inside kerogen nanopores.

While this study reveals pressure-dependent wettability trends of kerogen, limitations arise from its focus on homogeneous Type II-D models under fixed thermal-maturity conditions. Kerogen exhibits maturity-dependent composition (e.g., Type II-A to II-D) and nanoscale surface roughness-factors critical to fluid interactions but not yet incorporated. Future work should focus on the effects of surface roughness and kerogen maturity. A broad range thermo-pressure regimes (50-150 MPa, 300-400 K) is also suggested to explore the wettability behaviors covering the extreme subsurface environments. In addition, the validity of YL equation is only proved by one pore size in this work. In future, the applicability of the Young-Laplace equation should be rigorously tested at varying conditions including pore size, mineral types, and gas species.

Acknowledgements

This study was supported by the National Science Foundation of China (52404048) and the Science Research Project of Hebei Education Department (BJ2025116). This research was enabled in part by the support of the Digital Research Alliance of Canada (alliancecan.ca).

Conflict of interest

The authors declare no competing interest.

References

Alavi, S., Ripmeester, J., and Klug, D. Molecular-dynamics study of structure II hydrogen clathrates. The Journal of Chemical Physics, 2005, 123(2): 024507.

Alhamad, F., Sedev, R., Ali, M., et al. Effect of methyl orange on the hydrogen wettability of sandstone formation for enhancing the potential of underground hydrogen storage. Energy & Fuels, 2023, 37(8): 6149-6157.

Alinejad, A., and Dehghanpour, H. Evaluating porous media wettability from changes in Helmholtz free energy using spontaneous imbibition profiles. Advances in Water Resources, 2021, 157: 104038.

Al-Yaseri, A., Yekeen, N., Mahmoud, M., et al. Thermodynamic characterization of H_2-brine-shale wettability: Implications for hydrogen storage at subsurface. International Journal of Hydrogen Energy, 2022, 47(53): 22510-22521.

Bussi, G., Donadio, D., and Parrinello, M. Canonical sampling through velocity rescaling. The Journal of Chemical Physics, 2007, 126(1): 014101.

Chalmers, G. R., and Bustin, R. M. A multidisciplinary approach in determining the maceral (kerogen type) and mineralogical composition of Upper Cretaceous Eagle Ford Formation: Impact on pore development and pore size distribution. International Journal of Coal Geology, 2017, 171: 93-110.

Chow, Y. F., Maitland, G. C., and Trusler, J. M. Interfacial tensions of (H_2O+H_2) and (H_2O+ CO_2+H_2) systems at temperatures of (298-448) K and pressures up to 45 MPa. Fluid Phase Equilibria, 2018, 475: 37-44.

Essmann, U., Perera, L., Berkowitz, M. L., et al. A smooth particle mesh Ewald method. The Journal of Chemical Physics, 1995, 103(19): 8577-8593.

Hagler, A., Lifson, S., and Dauber, P. Consistent force field studies of intermolecular forces in hydrogen-bonded crystals. 2. A benchmark for the objective comparison of alternative force fields. Journal of the American Chemical Society, 1979, 101(18): 5122-5130.

Hashemi, L., Glerum, W., Farajzadeh, R., et al. Contact angle measurement for hydrogen/brine/sandstone system using captive-bubble method relevant for underground hydrogen storage. Advances in Water Resources, 2021, 154: 103964.

Huang, F., Yang, Y., Kang, S., et al. Microscopic insights into water wetting behaviors and physical origin on α-quartz exposed to varying underground gas species. Chemical Engineering Journal, 2024, 498: 155128.

Huhtamäki, T., Tian, X., Korhonen, J. T., et al. Surface-wetting characterization using contact-angle measurements. Nature Protocols, 2018, 13(7): 1521-1538.

Iglauer, S., Ali, M., and Keshavarz, A. Hydrogen wettability of sandstone reservoirs: Implications for hydrogen geo-storage. Geophysical Research Letters, 2021, 48(3): e2020GL090814.

Izadi, S., Anandakrishnan, R., and Onufriev, A. V. Building water models: A different approach. The Journal of Physical Chemistry Letters, 2014, 5(21): 3863-3871.

Jagadisan, A., and Heidari, Z. Molecular dynamic simulation of the impact of thermal maturity and reservoir temperature on the contact angle and wettability of kerogen. Fuel, 2022, 309: 122039.

Kadaoluwa Pathirannahalage, S. P., Meftahi, N., Elbourne, A., et al. Systematic comparison of the structural and dynamic properties of commonly used water models for molecular dynamics simulations. Journal of Chemical Information and Modeling, 2021, 61(9): 4521-4536.

Kirkwood, J. G., and Buff, F. P. The statistical mechanical theory of surface tension. The Journal of Chemical Physics, 1949, 17(3): 338-343.

Krishnamurthy, P. G., DiCarlo, D., and Meckel, T. Geologic heterogeneity controls on trapping and migration of CO_2. Geophysical Research Letters, 2022, 49(16): e2022GL099104.

Kuthe, S., Boström, M., Chen, W., et al. Exploring Wettability of Liquid Iron on Refractory Oxides with the Sessile Drop Technique and Density Functional-Derived Hamaker Constants. ACS Applied Materials & Interfaces, 2025, 17(10): 16173-16186.

Lander, L. M., Siewierski, L. M., Brittain, W. J., et al. A systematic comparison of contact angle methods. Langmuir, 1993, 9(8): 2237-2239.

Li, P., Nie, H., Zhang, J., et al. Characteristics and model of heterogeneous wettability in a marine-continental transitional shale reservoir: Insights from organic matter, minerals, and microstructure. Energy & Fuels, 2023, 37(9): 6450-6464.

Miyamoto, S., and Kollman, P. A. Settle: An analytical version of the SHAKE and RATTLE algorithm for rigid water models. Journal of Computational Chemistry, 1992, 13(8): 952-962.

Pan, B., Li, Y., Wang, H., et al. CO_2 and CH_4 wettabilities of organic-rich shale. Energy & Fuels, 2018, 32(2): 1914-1922.

Pan, B., Li, Y., Zhang, M., et al. Effect of total organic carbon (TOC) content on shale wettability at high pressure and high temperature conditions. Journal of Petroleum Science and Engineering, 2020, 193: 107374.

Pan, B., Ni, T., Zhu, W., et al. Mini review on wettability in the methane-liquid-rock system at reservoir conditions: Implications for gas recovery and geo-storage. Energy & Fuels, 2022, 36(8): 4268-4275.

Pang, W., and Jin, Z. Revisiting methane absolute adsorption in organic nanopores from molecular simulation and Ono-Kondo lattice model. Fuel, 2019, 235: 339-349.

Potoff, J. J., and Siepmann, J. I. Vapor-liquid equilibria of mixtures containing alkanes, carbon dioxide, and nitrogen. AIChE Journal, 2001, 47(7): 1676-1682.

Qin, C., Jiang, Y., Zhou, J., et al. Influence of supercritical CO_2 exposure on water wettability of shale: Implications for CO_2 sequestration and shale gas recovery. Energy, 2022, 242: 122551.

Ren, Q., Chen, G., Yan, W., et al. Interfacial tension of (CO_2+CH_4)+water from 298 K to 373 K and pressures up to 30 MPa. Journal of Chemical & Engineering Data, 2000, 45(4): 610-612.

Sanchouli, N., Babaei, S., Kanduc, M., et al. Wetting behavior of kerogen surfaces: Insights from molecular dynamics. Langmuir, 2024, 40(11): 5715-5724.

Scocchi, G., Sergi, D., D'Angelo, C., et al. Wetting and contact-line effects for spherical and cylindrical droplets on graphene layers: A comparative molecular-dynamics investigation. Physical Review E, 2011, 84(6): 061602.

Suekuni, M. T., Craddock, P. R., Douglas, J. T., et al. Critical practices for the preparation and analysis of kerogen. Energy & Fuels, 2022, 36(16): 8828-8843.

Tempra, C., Ollila, O. S., and Javanainen, M. Accurate simulations of lipid monolayers require a water model with correct surface tension. Journal of Chemical Theory and Computation, 2022, 18(3): 1862-1869.

Ungerer, P., Collell, J., and Yiannourakou, M. Molecular modeling of the volumetric and thermodynamic properties of kerogen: Influence of organic type and maturity. Energy & Fuels, 2015, 29(1): 91-105.

Van Der Spoel, D., Lindahl, E., Hess, B., et al. GROMACS: Fast, flexible, and free. Journal of Computational Chemistry, 2005, 26(16): 1701-1718.

Wang, C., Zhao, Y., Wu, R., et al. Shale reservoir storage of hydrogen: Adsorption and diffusion on shale. Fuel, 2024a, 357: 129919.

Wang, S., Gu, Z., Guo, P., et al. Comparative laboratory wettability study of sandstone, tuff, and shale using 12-MHz NMR T1-T2 fluid typing: insight of shale. SPE Journal, 2024b, 29(09): 4781-4803.

Yan, Z., Wang, F., Liu, Y., et al. Effects of CO_2 pressure on the dynamic wettability of the kerogen surface: Insights from a molecular perspective. Applied Surface Science, 2025: 162822.

Yang, Y., Nair, A. K. N., Zhu, W., et al. Molecular perspectives of interfacial properties of the hydrogen + water mixture in contact with silica or kerogen. Journal of Molecular Liquids, 2023, 385: 122337.

Young, T. An essay on the cohesion of fluids. Philosophical Transactions of the Royal Society of London, 1805, (95): 65-87.

Zheng, R., Germann, T. C., Huang, L., et al. Driving mechanisms of quartz wettability alteration under *in-situ* H_2 geo-storage conditions: Role of organic ligands and surface morphology. International Journal of Hydrogen Energy, 2024, 59: 1388-1398.

Zhou, J., Zhang, J., Yang, J., et al. Mechanisms for kerogen wettability transition from water-wet to CO_2-wet: Implications for CO_2 sequestration. Chemical Engineering Journal, 2022, 428: 132020.